ARTICLE

BIOTECHNOLOGY and BIOENGINEERING

A Tissue-Engineered Model of the Intestinal Lacteal for Evaluating Lipid Transport by Lymphatics

J. Brandon Dixon,[1,2] Sandeep Raghunathan,[1] Melody A. Swartz[1,2,3]

[1]Institute of Bioengineering, School of Life Sciences, École Polytechnique Fédérale de Lausanne (EPFL), CH-1015 Lausanne, Switzerland; telephone: +41 21 693 9686; fax: +41 21 693 9670; e-mail: melody.swartz@epfl.ch

[2]Department of Biomedical Engineering, Northwestern University, Evanston, Illinois

[3]Institute of Chemical Sciences and Engineering, School of Basic Sciences, EPFL, Lausanne, Switzerland

Received 4 September 2008; revision received 21 February 2009; accepted 20 March 2009

Published online 1 April 2009 in Wiley InterScience (www.interscience.wiley.com). DOI 10.1002/bit.22337

ABSTRACT: Lacteals are the entry point of all dietary lipids into the circulation, yet little is known about the active regulation of lipid uptake by these lymphatic vessels, and there lacks in vitro models to study the lacteal—enterocyte interface. We describe an in vitro model of the human intestinal microenvironment containing differentiated Caco-2 cells and lymphatic endothelial cells (LECs). We characterize the model for fatty acid, lipoprotein, albumin, and dextran transport, and compare to qualitative uptake of fatty acids into lacteals in vivo. We demonstrate relevant morphological features of both cell types and strongly polarized transport of fatty acid in the intestinal-to-lymphatic direction. We found much higher transport rates of lipid than of dextran or albumin across the lymphatic endothelial monolayer, suggesting most lipid transport is active and intracellular. This was confirmed with confocal imaging of Bodipy, a fluorescent fatty acid, along with transmission electron microscopy. Since our model recapitulates crucial aspects of the in vivo lymphatic–enterocyte interface, it is useful for studying the biology of lipid transport by lymphatics and as a tool for screening drugs and nanoparticles that target intestinal lymphatics.

Biotechnol. Bioeng. 2009;103: 1224–1235.

KEYWORDS: chylomicron; enterocyte; Caco-2; in vitro; fatty acid; Bodipy

Introduction

Lymphatic vessels are best studied for their roles in maintaining tissue fluid balance and in immune cell trafficking, but in addition, lymphatics are central to the transport of dietary lipid from the gut. In the small intestine, enterocytes reesterify the majority of free fatty acids (FFAs) absorbed from the lumen of the gut into triacylglycerols which are then incorporated into chylomicrons (Tso and Balint, 1986) and secreted basally to be picked up solely by lacteals, which are blind-ended lymphatic vessels in the center of each villus (Azzali, 1982; Schmid-Schönbein, 1990). Since the lymphatic vessels are the first tissue that chylomicrons encounter, as they are too large to be taken up by the surrounding blood capillaries (Tso and Balint, 1986), it is likely that lymphatic endothelium may actively regulate the transport and processing of dietary lipid; however, little is known about the biology governing lipid transport and metabolism by lymphatics. Nearly all in vivo studies of the synthesis of intestinal lipoproteins have relied on lymphatic drainage for the collection of chyle to study enterocyte assembly of lipids (Hayashi et al., 1990, 2002; Osada et al., 1994), yet it is difficult with these techniques to identify the specific contributions of lymphatics and differentiate them from those of enterocytes.

Lymphatic transport in the intestine, like in other locations throughout the body, is likely to be highly sensitive to fluid forces in the interstitium. For example, modulating tissue hydration of the interstitial matrix was shown to have profound effects on chylomicron transport presumably by altering lymph flow (Tso et al., 1985). Lacteals themselves also seem to have the capacity to physically adapt to a change in the load placed upon the vessel as it has been observed that lacteals alter their morphology in response to fasting and feeding (Habold et al., 2007). It remains to be determined, however, exactly how lymphatics actively regulate lipid uptake, or if responses by lymphatics such as these are merely reactions to changes

Correspondence to: M.A. Swartz

Contract grant sponsor: NIH
Contract grant number: HI075217; K99 KHL091133A
Contract grant sponsor: Whitaker International Scholars Fellowship

in the interstitial fluid forces. One recent study suggested that there may be some active regulation of lipid metabolism by lymphatic endothelium, although direct mechanisms remain elusive. It was found that mice with lymphatic developmental abnormalities due to a heterozygous mutation in Prox-1, which regulates lymphatic lineage commitment, develop adult-onset obesity as a result of leaky lymphatic vessels due to a loss of vessel integrity (Harvey et al., 2005). In addition, there have been several other recent editorials, short papers, and reviews that have alluded to or commented on the possible connection that might exist between lipid homeostasis and lymphatic function (Harvey, 2008; Rockson, 2004; Rosen, 2002; Ryan, 2006). The above-mentioned correlations between lymphatic function and lipid transport and metabolism remain largely phenomenological, primarily due to the lack of an experimental in vitro model that accurately recapitulates lipid transport from the enterocyte to the lacteal.

While some in vivo models exist [e.g., TEM studies (Azzali, 1982) or the lymph-fistula rat model (Hayashi et al., 1990)], they are limited in their preparation difficulty as well as ability to differentiate the lymphatic response to lipid from the immune response due to the close correlation between inflammation and lipid accumulation (Rutkowski et al., 2006). An in vitro model is needed to study human cells, for high throughput experiments, and to tease out specific responses of lymphatics, as well as to precisely examine biological regulation of lipid transport, yet no in vitro model exists to the best of our knowledge. Here we develop and characterize an in vitro model of the enterocyte-lacteal interface for studies of lipid uptake and transport and demonstrate its usefulness as a tool for quantifying the functional transport of lipid by lymphatics. By incorporating Caco-2 cells that have undergone differentiation in a transwell system, extracellular matrix, and lymphatic endothelial cells (LECs), we have modified a well-established model of chylomicron assembly to absorb and secrete lipid in the form of chylomicrons and FFAs that can then be transported across LECs. In order to establish the usefulness of such a model for studying both lipid uptake and drug delivery (Porter et al., 2007; Trevaskis et al., 2008), we demonstrate its relevance to the in vivo environment and report baseline measurements of FFA and lipid transport through this in vitro model.

Materials and Methods

Cell Lines

Caco-2 cells (LGC Promochem, Middlesex, England) were expanded in high glucose DMEM (PAA, Pasching, Austria) supplemented with 20% FBS, 1% antibiotic-antimicotic mixture (both from Invitrogen, Carlsbad, CA). The media was changed every 2 days and the cells were not allowed to reach confluence before being passaged. The Caco-2 cells used in experiments were between passages 20 and 30. LECs were obtained through an isolation from human neonatal foreskins via immunomagnetic separation using the LEC marker LYVE-1 as described previously (Podgrabinska et al., 2002). The LECs were expanded in flasks that had been previously coated for 1 h with a collagen solution containing type I rat tail collagen (BD Biosciences, San Jose, CA) at a concentration of 50 μg/mL and 0.1% acetic acid (Sigma, St. Louis, MO). The cells were grown in EBM (Lonza, Basel, Switzerland) supplemented with 20% FBS, 1% Glutamax, 1% penicillin-streptomycin (all from Invitrogen), 25 μg/mL cyclic-AMP, and 1 mg/mL hydrocortisone acetate (both from Sigma). LECs were split before reaching confluence and were used in experiments between passages 7 and 10.

Coculture and Experimental Setup

Caco-2 cells were seeded at a density near confluence (1.5×10^5 cells/cm^2) onto the bottom of a 0.4 μm pore size transwell (Corning Life Sciences, Koolhovenlaan, The Netherlands) that had been coated with collagen using the same technique described above. The cells were given an hour to attach to the membrane before inverting the hanging transwells into a 12-well plate. The cells were treated with the same medium described above, and the medium was changed every 2 days until 21 days after the cells reached confluence, allowing for differentiation into an enterocyte phenotype (Pinto et al., 1983). Transepithelial electrical resistance (TER) measurements were made to ensure that a highly resistive cell layer had formed. The transwell insert was then coated with the previously mentioned collagen solution and seeded with LECs at a high density (10^5 cells/cm^2). The cells were cultured together with their respective media bathing each side of the transwell for 3 days. The media on both sides was then replaced with DMEM containing 2% FBS for 12 h before experiments on the culture model were performed. Unless specified otherwise, all transport studies were carried out in DMEM with 2% FBS, which was chosen to provide the cells with essential nutrients yet minimize the effect of serum on the experiments.

Immunofluorescence

To whole-mount stain mouse lacteals, a 5 cm segment of mouse small intestine was isolated from the proximal region and fixed overnight in 4% PFA at 4°C. After blocking, the tissues were treated with the respective primary antibodies, LYVE-1 at a dilution of 1:500 (Millipore, Billerica, MA) and CD31 at a dilution of 1:200 (BD Biosciences) overnight at 4°C in PBS containing 2% bovine serum albumin (PAA). The tissues were rinsed and then stained for 1 h at room temperature with the appropriate secondary antibody (Invitrogen) at a dilution of 1:200.

Transwell membranes were fixed for 15 min with 4% PFA at room temperature immediately after the collection of media samples for the plate reader, which occurs 6 h after the

addition of the tracer of interest. All in vitro staining presented here is representative of the cells at this 6 h time point. Antibody staining was performed using the same protocol as described above with VE-Cadherin (BD Biosciences) at a dilution of 1:50. Alexa-labeled phalloidin (Invitrogen) was added (diluted 1:50) with the secondary solution.

Scanning Electron Microscopy

Caco-2 cells were fixed in 2% glutaraldehyde (Sigma) for 2 h at various time points during their differentiation. They were then prepared for SEM by washing in Sorensen buffer solution (Labo-Moderne, Paris, France) and treating with 1% osmium tetroxide (Sigma) for 1 h. They were then dehydrated in a sequence from 25% to 100% ethanol, dried by CO_2 critical point, coated with 20 nm gold, and imaged with a JSM 6300F electron microscope equipped with the Mamiya 6×7 UHR (TMX120 ISO100) camera (Joel Ltd, Tokyo, Japan).

Transmission Electron Microscopy Preparation

Cells were fixed in freshly prepared fixative (2.5% glutaraldehyde, 2% paraformaldehyde) at 4°C for 4 h and then rinsed and stored overnight at 4°C in PBS. The following morning samples were washed 3× in cacodylate buffer (0.1 M, pH7.4) at 4°C. They were then postfixed in 1% osmium tetroxide and 1.5% potassium ferrocyanide in cacolydate buffer for 40 min. The solution was then changed out with 1% osmium tetroxide in cacolydate buffer and incubated for an additional 40 min. Cells were washed twice with distilled water and stained with 1% uranyl acetate for 40 min. The cells were washed again in distilled water and then dehydrated with washes of increasing ethanol concentration (1× 50%, 1× 70%, 2× 96%, 2× 100%). Cells were embedded in 1:1 solution of Durcapan and 100% ethanol for 30 min while rotating the sample. The solution was replaced with fresh Durcapan and samples were rotated for an additional 1 h. This step was repeated twice. Cells immersed in Durcapan were then placed in the oven at 65°C overnight to allow the resin to harden. The next day samples were sliced into 50 nm sections using a diamond knife and then mounted on grids for viewing later.

Permeability Measurements

The intestinal side of the transwell was treated with either 70 kDa Texas Red—dextran, 3 kDa Cascade Blue—dextran, FITC—albumin, or Bodipy FL C16, a fluorescently labeled 16 carbon chain fatty acid, (all from Invitrogen) or some combination thereof (Fig. 1A). In some cases, 1.6 mM oleic acid (OA) and 1.0 mM taurocholic acid (TC, both from Sigma) (OA/TC), which are known to promote chylomicron formation (Luchoomun and Hussain, 1999), were added to the intestinal side of the transwell. At 6 h, two 150 μL samples were collected from the lymphatic side of the transwells and their fluorescence was measured in a Safire2 plate reader (Tecan, Männedorf, Switzerland) and compared to a standard curve to estimate P_{eff} (μm/sec) using a previously established method (reviewed in Mehta and Malik, 2006; Michel and Curry, 1999). Briefly, effective permeability to a tracer was calculated as a function of the solute flux J_s (mg/sec), the concentration gradient ΔC (mg/mL), and the surface area of the monolayer S (cm^2):

$$P_{\text{eff}} = \frac{J_S}{\Delta C S}$$

After 6 h, the solute concentration on each side was determined by correlating the fluorescence reading with a standard curve, and J_s was determined by multiplying the concentration in the lower well by the medium volume (0.5 mL) and dividing by the time course of the experiment (6 h). Pilot experiments were performed in which samples were taken at multiple time points to ensure that the flux was linear over the duration of the experiment; we chose one 6-h time-point rather than multiple time-points because of potential error due to convection and mixing from multiple sampling.

To measure transport across LECs alone, we treated Caco-2 cells with OA/TC and Bodipy as above, and collected the secretions after 12 h. The secretions from multiple wells were pooled together and diluted in DMEM containing 2% FBS and were placed on the LECs for 1 h. This shorter time point for LECs alone was chosen because we found that the transport of Bodipy-containing secretions across the LEC monolayer was much faster than Bodipy transport across the two-cell model.

Gel Filtration Chromatography

To separate size fractions containing secreted proteins from the two-cell model, we used gel filtration chromatography (GFC) to size-separate lipoproteins from serum (Orth et al., 1998). Specifically, we layered two Sepherose gels in a 1 cm wide column: the lower 55% of the column height was filled with Sepherose CL-6B and the upper 45% was filled with Sepherose CL-2B (both from Sigma) for a total height of either 16 or 19 cm. A sample volume of 0.5 mL was loaded on the top of the column and filtered at a flow rate of approximately 750 μL/min (filtration buffer: 145 mM NaCl, 0.21 mM Na_2EDTA, and 25 mM Tris, pH 7.5), which was provided by a constant pressure head. Forty-eight fractions were collected in 0.5 mL volumes and saved for analysis. Two hundred microliters samples were extracted from each sample and the relevant fluorescence was read on a Safire2 plate reader. Samples containing Texas red-labeled albumin (10 μg/mL, Invitrogen) or 200 nm beads (10 μg/mL, Invitrogen) were run through the column as size standards.

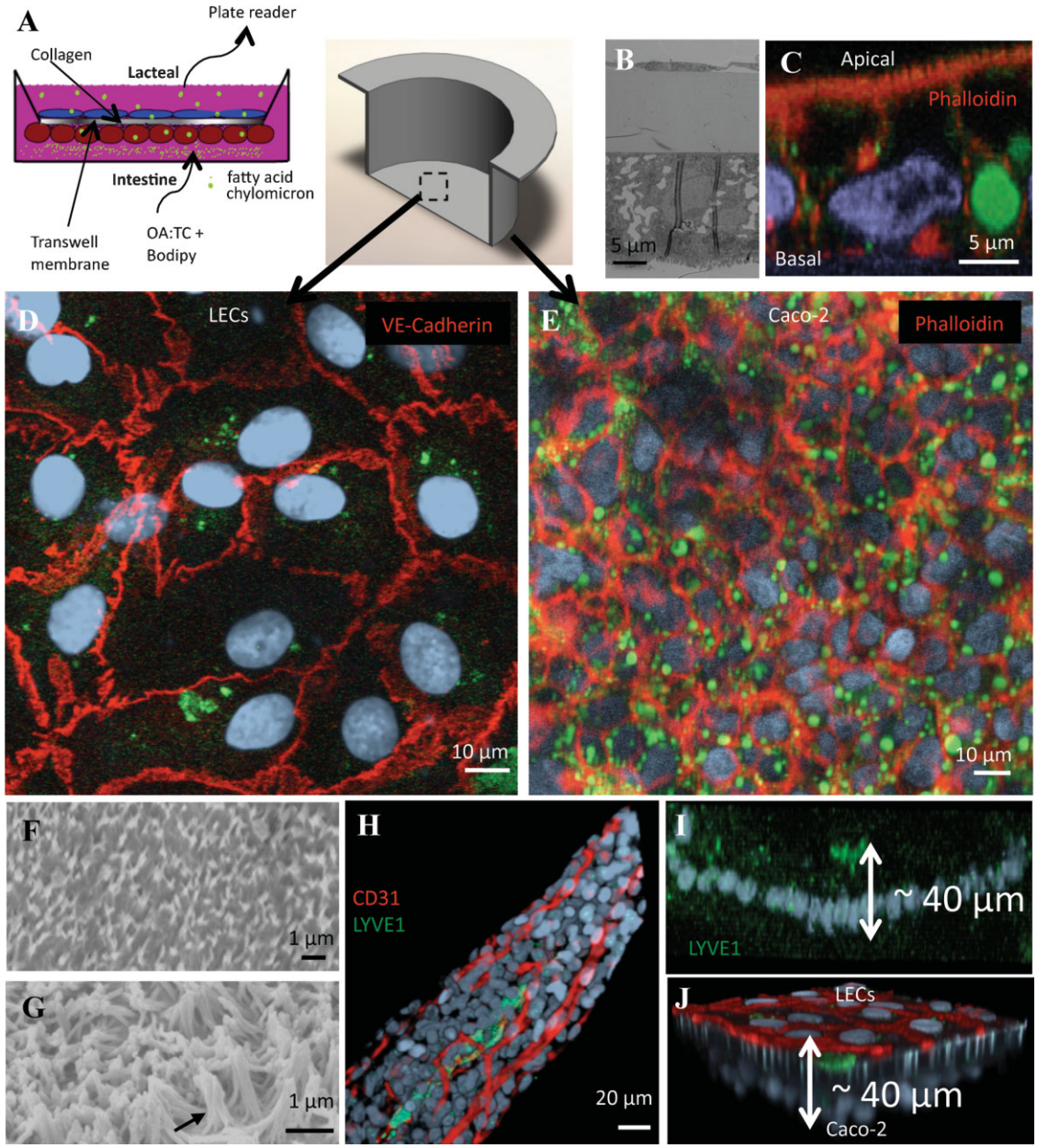

Figure 1. The in vitro model recapitulates the morphology of the lymphatic—enterocyte interface. **A**: Schematic and CAD drawing of the transwell system. **B**: TEM image of an orthogonal slice of the transwell showing the relative thickness of each layer: Caco2 cells (~20 µm), transwell membrane (~12 µm), LECs (~ 5 µm). **C**: Caco-2 cells develop columnar morphology with nuclei located near the basal surface of the cell; f-actin is stained with phalloidin (red), nuclei with DAPI (blue), and fatty acid with Bodipy (green). **D**: LECs, plated on the top of the insert, show typical morphology and cell–cell junctions (VE-Cadherin, red), and contain fatty acid-containing vesicles (Bodipy, green). **E**: The Caco-2 cell layer, plated on the bottom of the transwell, contains tightly packed cells (phalloidin, red; nuclei, blue) containing numerous Bodipy-containing vesicles (green). **F** and **G**: Scanning electron micrographs of the Caco2 cell surface after 2 days (F) or 3 weeks (G) of culture showing the formation of microvilli (black arrow) over time characteristic of enterocyte differentiation. **H**: 3-D reconstruction of confocal slices of a mouse intestinal villus with a lymphatic vessel in the center; nuclei are stained with DAPI (light blue), blood vessels with CD-31 (red), and lymphatic endothelium with LYVE-1 (green). **I**: Cross-section of a lacteal exhibits the lacteal located in the center of the villus, perpendicular to the imaging plane; the distance between the apical side of the enterocyte and the basal side of the lymphatic is approximately 40 µm. **J**: Side view of the 2-cell model system showing a similar enterocyte—lymphatic distance as that seen in vivo.

For samples that had been treated with OA/TC (but not Bodipy), the secretions were incubated with C6-NBD-ceramide (1 µg/mL, Invitrogen) for 30 min to allow the probe to be incorporated into the lipoproteins before being run through the column.

Quantification of Total Lipid

In the GFC size-separated fractions that labeled positively with NBD, we used an extraction method to measure total lipid (Amenta, 1970). Three hundred microliters of our

sample was added to 1 mL of a 45% chloroform, 55% methanol solution and mixed vigorously for 5 min. The sample was allowed to stand for 1 h, mixing again every 20 min. 2.7 mL of 5 mg/mL $CaCl_2$ dissolved in water was added and shaken vigorously for 5 min. The sample was spun at 1,000*g* to separate the phases and 200 μL was extracted from the bottom phase containing the lipid and chloroform. This sample was evaporated at 110°C and resuspended into 1 mL of a dichromate solution (200 mg of $K_2Cr_2O_7$ dissolved into 2 mL of water and the diluted with 40 mL of H_2SO_4). Forty microliters of this sample was diluted in 160 μL water and its absorbance at 430 nm was measured with a plate reader. A standard curve was made by running samples of LDL at a known concentration (Lee BioSolutions, St. Louis, MO) of various dilutions through the same procedure. This curve was used to calculate the total lipid in each fraction based on the absorbance reading at 430 nm.

Animal Experiments

All protocols were approved by the Veterinary Authorities of the Canton Vaud according to Swiss law (protocol no. 1952). Mice were administered 300 μL of a lipid cocktail containing water (100 μL), olive oil (100 μL), cream (35% milk fat) (100 μL), 70 kDa dextran (30 μg), and Bodipy FL C16 (30 μg) via gavage. After 1 h the animal was anesthetized with a subcutaneous injection of ketamine (3.75 mg/100 g body weight) and xylazine (0.75 mg/100 g body weight). Supplemental doses of the anesthetic were given as needed. An abdominal incision was made and a loop of the small intestine was exteriorized through the incision and gently positioned over a semicircular viewing pedestal on a Plexiglas preparation board designed to supply the vessel with crucial nutrients and maintain temperature. A lymphatic vessel was identified by its morphology and/or the presence of Bodipy and centered over an optical window in the preparation board. The exteriorized tissue was perfused with an albumin physiological salt solution (in mM): 145.00 NaCl, 4.7 KCl, 2.0 $CaCl_2$, 1.17 $MgSO_4$, 1.2 NaH_2PO_4, 5.0 dextrose, 2.0 sodium pyruvate, 0.02 EDTA, 3.0 MOPS, and 10g/L bovine serum albumin (all from Sigma) that was pre-warmed to 38°C, and the pH adjusted to 7.4. The temperature of the exteriorized tissue and the animal's core was maintained at 36–38°C (Dixon et al., 2006). Temperature was monitored with a thermocouple probe throughout the experiment. The mesenteric lymphatics were imaged under a Leica MZ16 FA fluorescence-equipped stereomicroscope.

Statistics

All statistics were performed using SPSS (Chicago, IL). Statistical significance between groups was established using one-way ANOVA followed by a Tukey post-hoc test to correct for multiple comparisons.

Results and Discussion

Replicating In Vivo Morphology

The first goal was to recapitulate key morphological and functional features of the enterocyte-lacteal interface in vitro, therefore we optimized and characterized features relevant to lipid and FFA transport across LECs. Caco-2 cells were used since they can be differentiated into cells with similar morphology and function to enterocytes, the epithelial cell responsible for lipid absorption and lipoprotein assembly in the intestine, and are well-characterized for lipoprotein synthesis (Levy et al., 1995; Luchoomun and Hussain, 1999; Pinto et al., 1983). However, there are a few noteworthy differences between enterocytes and Caco-2 cells. Caco-2 cells synthesize both ApoB-100 (present in the liver) and ApoB-48 (intestinal form); however, when cultured on transwells and allowed to differentiate, the ApoB-48/ApoB-100 ratio is maximized. Caco-2 cells also express much lower levels of intestinal fatty acid binding protein (I-FABP) than enterocytes, although I-FABP is not necessary for Caco-2 cells to absorb and metabolize long chain fatty acids (Darimont et al., 1998). In addition, synthesis of fat via the monoacylglycerol pathway in Caco-2 cells is much lower than that observed in vivo (Levy et al., 1995; Trotter and Storch, 1993). However, since our primary interest is to utilize the ability of Caco-2 cells to assemble and secrete chylomicrons from a source of fatty acids, it is a useful model cell line for this study. Human dermal LECs were used because of a lack of a human lacteal cell line; however, there has not yet been any evaluation of how dermal versus intestinal lymphatic capillaries differ.

By staggering the timing of cell seeding, Caco-2 cells are allowed to first differentiate and develop their enterocyte phenotype, before LECs are added to the transwell. When cultured together in the transwell system (Fig. 1A), LECs and Caco-2 cells formed separate confluent monolayers on opposite sides of the membrane with the membrane itself separating the cells by approximately 12 μm (Fig. 1 B). The Caco-2 cells developed a typical columnar morphology with the nucleus located near the basal surface of the cell (Fig. 1C), and TER measurements verified a tight junctional integrity (data not shown). Both cell types appeared to form typical morphologies (Fig. 1D and E). VE-cadherin staining on LECs revealed a discontinuous expression pattern (Fig. 1D) characteristic of initial lymphatics (Baluk et al., 2007), and no apparent difference was seen in response to chylomicron secretion by Caco-2 cells. This is consistent with previous in vivo SEM studies on lipid uptake into lacteals in which the junctions between adjacent lymphatic endothelial cells of the rat lacteal remain closed during both fasting and feeding conditions (Azzali, 1982; Dobbins and Rollins, 1970).

The model setup allows for fatty acid and lipid transport from the apical side of the Caco-2 cells to the apical side of the LEC monolayer to be quantified in a plate reader and for lipid trafficking through the cells to be imaged with confocal

microscopy. While the green fluorescent Bodipy can be seen in vesicle-like compartments in both cell types (Fig. 1D and E), Bodipy-containing vesicles were more predominant in the intestinal cells, as these cells provide the rate-limiting step in fatty acid uptake into lymphatics (Tso and Balint, 1986). Microvilli on the Caco-2 cells, which further demonstrated enterocyte differentiation as characteristic of the brush border organization seen in vivo (Pinto et al., 1983), while not present after 2 days of culture (Fig. 1F) were seen under scanning electron microscopy (SEM) after being kept in culture for 3 weeks (Fig. 1G).

Since the main focus of this model is to study transport, it is essential that the transport distance between the two physiologic compartments is similar to what occurs in vivo. In vivo, enterocytes and blood vessels surround the lacteal in the center of each intestinal villus (Fig. 1H), and the distance between the lymphatic and the apical surface of the enterocyte is approximately 40 μm (Fig. 1I). In our in vitro model, the distance between the apical side of the enterocytes and the apical side of the LECs was approximately 40 μm (Fig. 1J), of which the insert contributed 12 μm.

Replicating In Vivo Function

To assess functionality, we adapted for the mouse a preparation used in previous studies of rat mesenteric lymphatic function (Dixon et al., 2005, 2006, 2007) and imaged Bodipy uptake into lymphatic vessels in the anesthetized mouse. When the same volume and concentration of Texas Red-conjugated dextran (70 kDa) was co-delivered with Bodipy, Bodipy was seen to be transported through the intestine and taken up by lymphatics (Fig. 2A), while dextran was not visible in any tissues outside of the intestine (Fig. 2B). Multiple images of the intestine were taken at various exposure times to ensure that the differences seen were not due to differences in the quantum yield of the dye (data not shown). The differences between the uptake of dextran and Bodipy into lymphatics can be clearly seen in higher magnifications of individual vessels 20 μm in diameter (Fig. 2C–E).

Likewise, in our in vitro model, we found that only Bodipy was transported across to the lymphatics, while Caco-2 cells prevented the transport of dextran and albumin (Fig. 2F). We also quantified transport for a range of dextran sizes (10, 70, and 2,000 kDa) that were fluorescently labeled. While all three were transported through LECs alone to varying degrees, no transport was detected through the two-cell layer or through Caco-2 cells (data not shown) within the timeframe of the experiment. When comparing the transport of dextran and albumin through each cell type individually and through the two-cell model, it was clear that the Caco-2 cells provided the main barrier to transport of these two molecules. However, the opposite was true for Bodipy as Caco-2 cells modify Bodipy to be transported more effectively through LECs than when it is added to LECs alone under the same 2% serum conditions (Fig. 2F). This was further confirmed by adding secretions from Caco-2 cells, which had been previously treated with Bodipy, onto LECs. Bodipy in this form, was transported over 50 times more rapidly than when it was added directly to LECs and was also transported much more effectively than fluorescently labeled albumin (Fig. 2G).

For certain experiments it would be advantageous to grow the two cell types separately and characterize the transport of Bodipy through each compartment separately (e.g., to chemically block specific mechanisms of transport in LECs without affecting the transport through the enterocyte layer or vice versa). By collecting secretions from Caco-2 cells that have been treated with Bodipy and OA/TC, and then placing this media directly onto LECs, we could calculate the permeability of LECs alone to these secretions. When the two different cell types were cultured separately and transport of Bodipy was measured in each stage individually, the sum of the resistance ($1/P_{\text{eff}}$) to Bodipy transport of each cell compartment should be equal to the resistance of Bodipy transport through the two cell model, thus the total permeability of two compartments in series with known permeability can be calculated with the following equation:

$$\frac{1}{P_{\text{eff}}} = \frac{1}{P_1} + \frac{1}{P_2}$$

When the total permeability of Caco-2 cells and LECs placed in series was calculated from the experimental permeability measured for each cell type individually, the result agreed well with the effective permeability measured experimentally in the two-cell model (Fig. 2H).

Previous work characterized the uptake of Bodipy Fl C_{16} by Caco-2 cells (Thumser and Storch, 2007) and showed that the probe targeted the endoplasmic reticulum/golgi apparatus and that no localization of the probe was found in the lysosome after 15 min, suggesting that the probe would be targeted for subsequent use as an energy substrate for esterification into phospholipids and triacylglycerols that would then be incorporated into lipoproteins. In order to determine what size range of proteins the Bodipy was being incorporated into, we performed gel filtration chromatography (GFC). Since FFAs are known to bind albumin, we compared serum-free conditions with 2% serum-containing medium when examining Bodipy transport across the two-cell model. In serum-free conditions, the Bodipy elutes with a much later fraction than albumin, suggesting that Bodipy was associated with smaller molecules (Fig. 3A). However, in 2% serum, most of the Bodipy elutes in the same fraction as albumin, while a small peak is seen in an earlier fraction (arrow in Fig. 3A), suggesting that at least some of the Bodipy is incorporated into a larger lipoprotein such as a chylomicron. It is important to note that the Bodipy-containing Caco-2 secretions, even if mostly bound albumin, were transported across the LEC monolayer ten times more rapidly than was albumin (Fig. 2F–G),

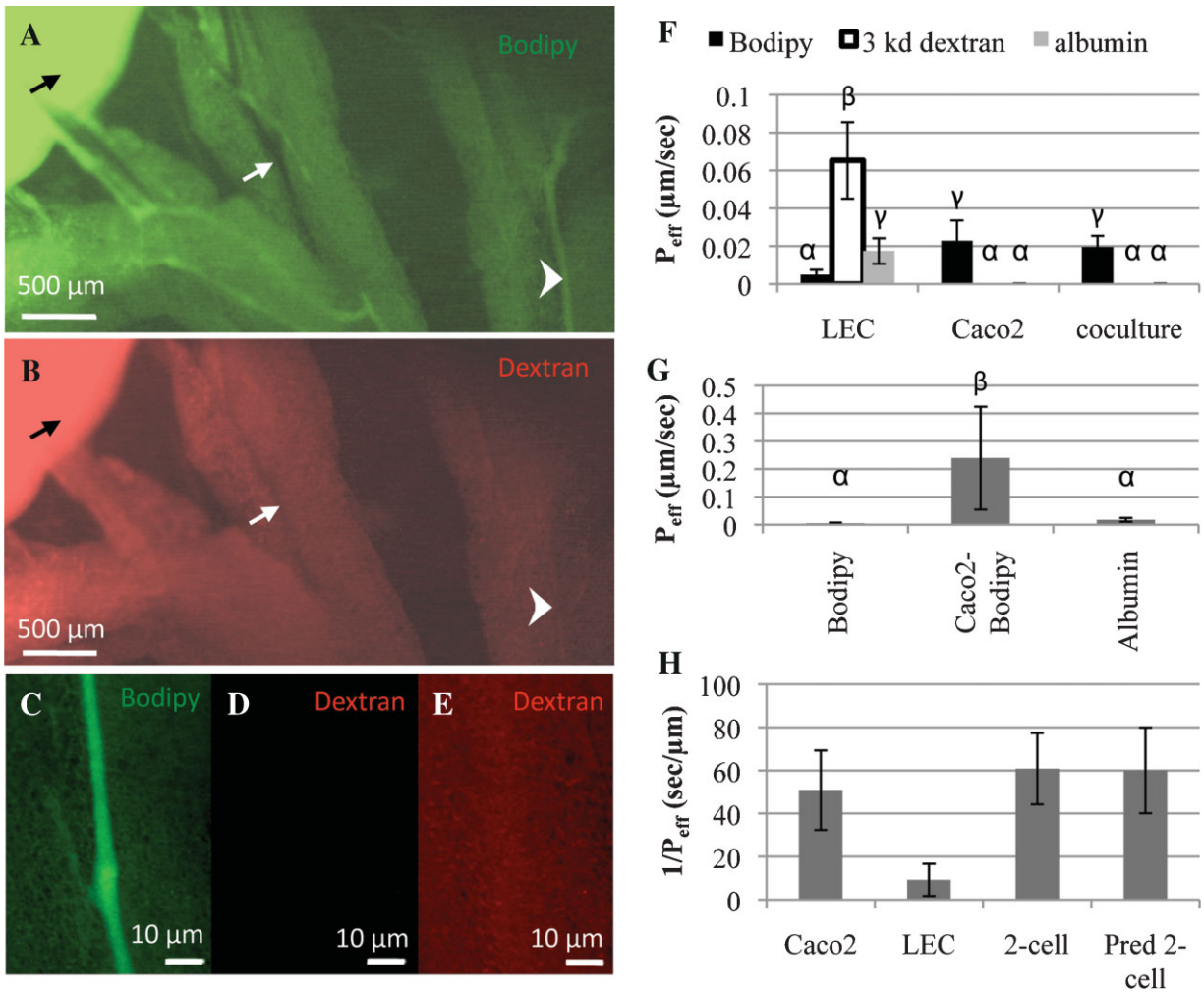

Figure 2. The in vitro model recapitulates key features of in vivo lipid absorption function. **A**: Bodipy (green) is specifically taken up from the intestine (black arrow) into lymphatic vessels (arrowhead) and not blood vessels (white arrow) after oral delivery. **B**: 70 kDa Texas Red—dextran, while visible in the intestine (black arrow) after oral delivery, is not visible in the lymphatics or the blood vessels. **C**: Enlarged region from (A) as indicated, where Bodipy can clearly be seen inside the lymphatic vessel. **D**: Enlarged region from (B), taken at the same exposure time as (C), shows that dextran is not visible in the Bodipy-containing lymphatic. **E**: Enlarged region from (B) taken at six times the exposure time shows that the red fluorescence in the lymphatic vessel is indistinguishable from background fluorescence. **F**: Similar to the in vivo case, the two-cell model transports fatty acid much more rapidly than other proteins or large dextrans (bars not sharing the same letters are statistically significantly different, $P < 0.05$). In all cases, the tracer was added to the underside (Caco-2 apical side) of the insert and collected from the top (LEC apical side). **G**: Bodipy is transported much more effectively across a monolayer of LECs after it has been absorbed and secreted by Caco-2 cells (Caco2-Bodipy) first, which was achieved by adding Bodipy-containing Caco-2 secretions onto LECs, compared to when Bodipy is added directly to LECs ($P < 0.01$). **H**: The Caco-2 cell permeability to Bodipy and the LEC permeability to Caco-2 secreted Bodipy can be used to predict the permeability of the two-cell model to Bodipy (Pred 2-cell), which agrees well with experimental results (2-cell).

indicating that albumin-associated bodipy is transported differently across LECs than albumin.

To further demonstrate chylomicron secretion from the two-cell model, secretions from Caco-2 cells treated with OA/TC were labeled with C_6-NBD-ceramide, which is known to bind to lipoproteins (Hosken et al., 2005), filtered using GFC, and then the fluorescence of each fraction was measured with a plate reader. Lipoproteins were eluted similarly as 200 nm beads (Fig. 3B), indicating a size range consistent with chylomicrons. The total lipid in these fractions (8–13) was determined by extraction followed by incubation with a dichromate solution and absorbance reading as described in Materials and Methods Section. Much more lipid was found in OA/TC-treated Caco-2 cell secretions than without the OA/TC (Fig. 3C), which promotes chylomicron formation (Luchoomun and Hussain, 1999). Furthermore, when Pluronic L-81, a hydrophobic polymer known to inhibit the formation of large chylomicrons (Luchoomun and Hussain, 1999; Tso et al., 1980), was added to the solution at 1 µg/mL, no lipid was detected in fractions 8–10, while lipid was present in some of the later fractions (11–13); this indicated that the size range of the lipid-containing species was shifted to a smaller range upon addition of Pluronic L-81. It should be noted that the column used in Figure 3B and C was larger than that used for the data in Figure 3A, and thus albumin elution occurs at

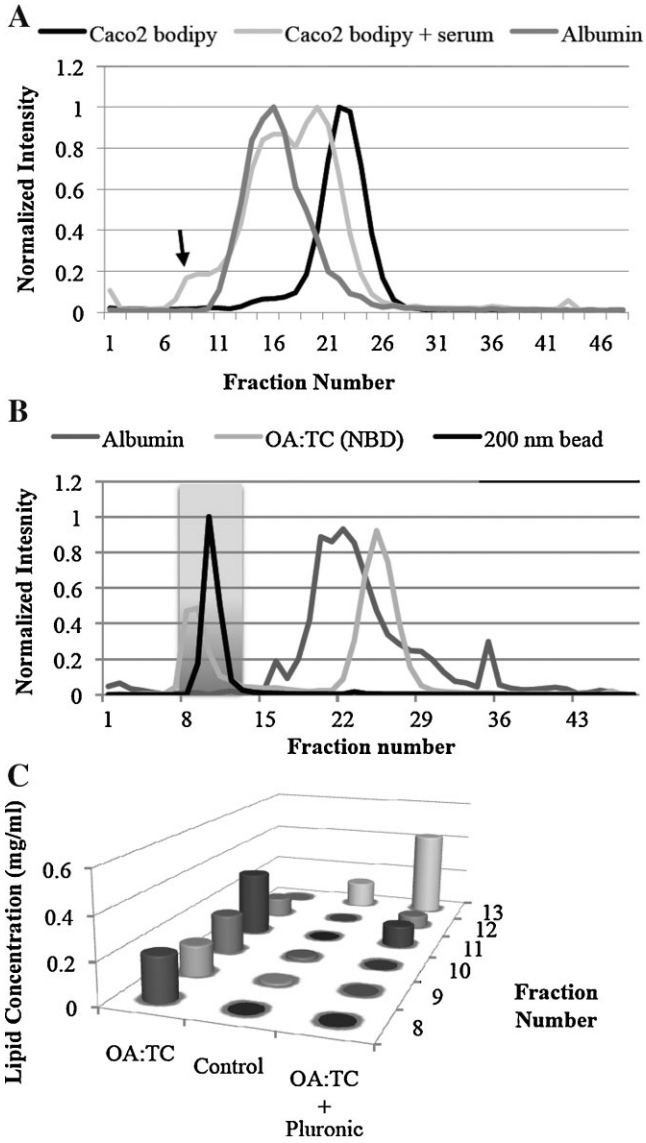

Figure 3. Bodipy is secreted by Caco-2 cells in both lipid-associated and albumin-associated species. **A**: Bodipy secreted by Caco-2 cells is contained in a lower size fraction than albumin when the experiment is carried out in serum-free conditions, but in 2% serum, the Bodipy elutes in higher size fractions, with the predominant fraction being that which contains albumin, suggesting albumin binding in the two-cell model. A smaller percentage of the Bodipy is associated with larger size fractions (arrow), indicating lipoprotein incorporation. **B**: OA/TC treated Caco-2 secretions contain lipoproteins labeled with NBD-ceramide (OA/TC (NBD)) that elute with 200 nm nanoparticles. **C**: OA/TC treated Caco-2 cells secrete substantially more lipid as compared to untreated cells in the fractions highlighted in (B), suggesting the formation of lipid-rich lipoproteins. The amount of lipid in the larger fractions is drastically reduced when Pluronic L81, a hydrophobic polymer known to interfere with the formation of large chylomicrons, is added to the OA/TC treated cells.

different fractions. Also, the second peak in the NBD sample corresponds to the free NBD remaining in the solution, as it corresponds to samples containing only NBD (data not shown).

Together, these findings suggest that most of the Bodipy transported across the two-cell model is associated with albumin, but a significant fraction is associated with larger lipid particles. Furthermore, it shows that lipid transport can be measured and manipulated across the model.

Lymphatic Transport of Bodipy Occurs Through Both Transcellular and Paracellular Pathways

Using confocal microscopy on the LEC monolayer, we observed fluorescent Bodipy both in cytoplasmic vesicles within the cell and associated with overlapping cell-cell junctions (Fig. 4A–C), as indicated by immunostaining for VE-cadherin (Fig. 4C), which controls permeability in both blood and lymphatic endothelium (Baluk et al., 2007; Dejana, 2004; Ng et al., 2004). This suggests that both transcellular and paracellular pathways may be used for Bodipy transport across LECs, although the vast majority of Bodipy was seen clearly within the cell boundaries. In these cases, Bodipy was often seen in vesicles that lined up in a chain-like fashion, and the size of these vesicles suggests the formation of vesiculo-vacuolar organelles or transendothelial channels (Fig. 4B) (Feng et al., 2002). It is uncertain whether the Bodipy observed within these cells was attached to albumin, incorporated into a lipoprotein, or bound to a fatty acid binding protein. Others have shown, as we have in Figure 2, that when delivered in vivo, Bodipy is taken up directly into lymphatics (Harvey et al., 2005). In addition to this, free fatty acids have been shown to be present in intestinal lymph after feeding (Beckett et al., 1981; Blomstrand and Dahlback, 1960; Papp and Makara, 1965), yet the importance or regulation of free fatty acid transport by lymphatics is unclear. Thus, Bodipy C16 is a potentially interesting probe to investigate more closely the mechanisms of free fatty acid transport by lymphatics and the role of albumin in this process.

Transport Is Polarized in the Enterocyte to Lymphatic Direction

In our in vitro model, we found that Bodipy transport was polarized in a physiologically relevant direction (Fig. 4D). Evidence of this polarization, which is characteristic of enterocyte-like differentiation of Caco-2 cells, was also seen with confocal imaging, where numerous Bodipy-containing vesicles were seen in the Caco-2 cells when transport was in the intestinal-to-lymphatic direction (Fig. 4E) but none were observed when concentration gradients were reversed (Fig. 4F). This is expected because the luminal side of enterocytes have numerous microvilli located at what is known as the brush border, which increases the surface area and enhances lipid absorption (Tso and Balint, 1986). This

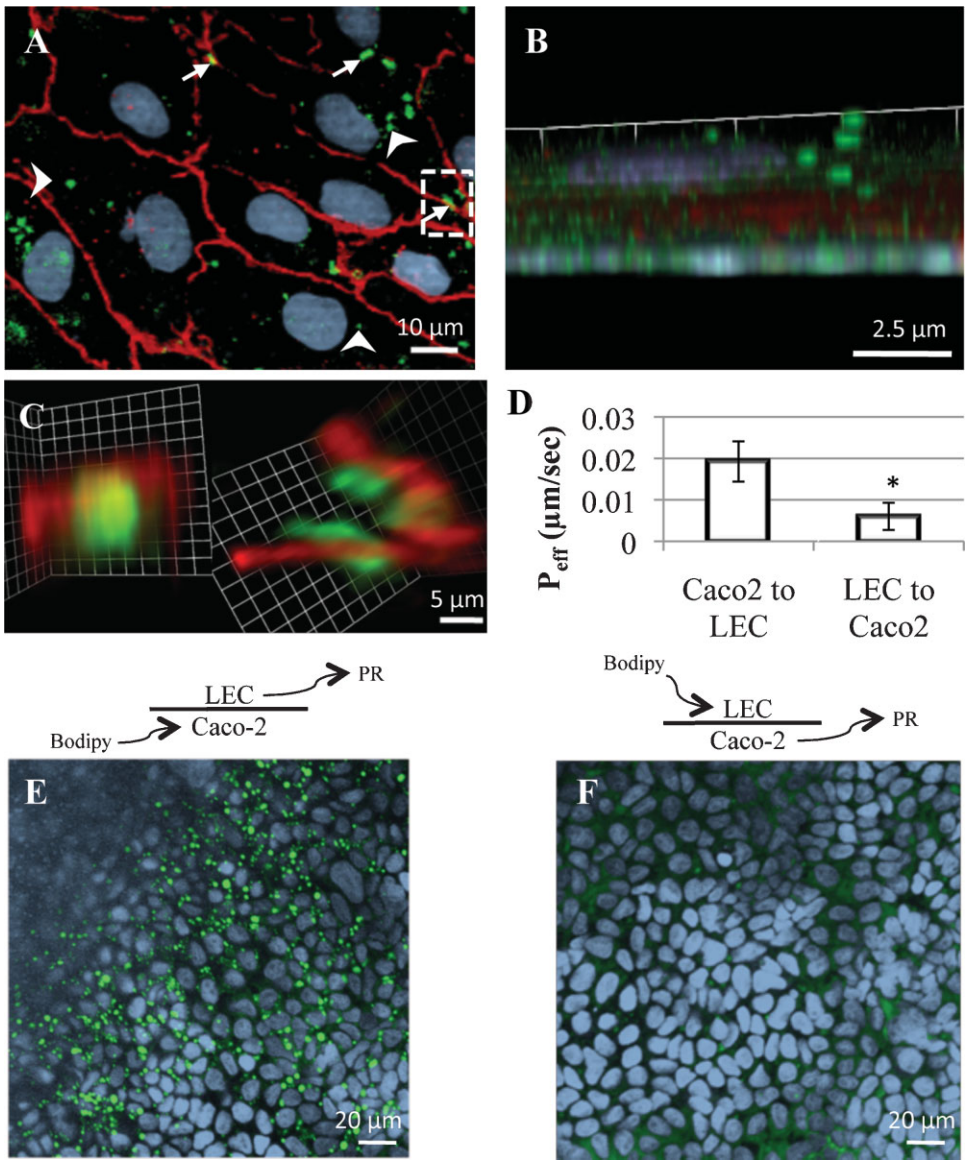

Figure 4. Bodipy is transported via both paracellular and transcellular pathways through LECs in vitro. All images show LECs on the underside of the culture insert membrane that were in coculture with Caco-2 cells treated with Bodipy and OA/TC. **A**: Maximum projection confocal image of LECs stained with VE-Cadherin (red) show Bodipy (green) being transported both transcellularly (arrowhead) and paracellularly (arrow). **B**: Cross-section of a single LEC stained with VE-Cadherin, showing Bodipy transcytosing through the cell via vesicles in a chain-like fashion. **C**: Enlarged view of the insert marked in (A) demonstrates Bodipy traversing through the cell and overlapping with VE-cadherin as shown from two different perspectives: perpendicular to the imaging plane (left) and parallel to the imaging plane (right). **D**: Effective permeability (P_{eff}) of the two-cell model to Bodipy was much higher when lipid is added to the Caco-2 side of the transwell as compared to the LEC side, demonstrating polarization of transport. **E**: Vesicles containing Bodipy (green) were observed inside the Caco-2 layer when Bodipy was added to the intestinal side of the co-culture model. **F**: Vesicles were absent from the Caco-2 cell layer when the same concentration of the probe was added to the LEC side of the co-culture model, demonstrating polarization in transport.

polarization of lipid transport is critical for model validation regarding its usefulness in lipid transport studies.

Lymphatic Transcytosis of Lipoproteins

Electron microscopy studies have demonstrated uptake of chylomicrons and other large particles into lymphatics in vivo via both transcellular and paracellular pathways (Azzali, 1982; Dobbins and Rollins, 1970; Feng et al., 2002), and here we demonstrate lipid transcytosis across LECs in vitro (Fig. 5). Using TEM of the two-cell model, we observed numerous lipid vesicles within LECs in the two-cell model that were treated with OA/TC to promote chylomicron formation by Caco-2 cells (Fig. 5A–C). Vesicles were often seen fusing with the cell membrane on both the apical side as they took up lipid and the basal side as they released it (Fig. 5A and B). It is interesting to note that these vesicles are

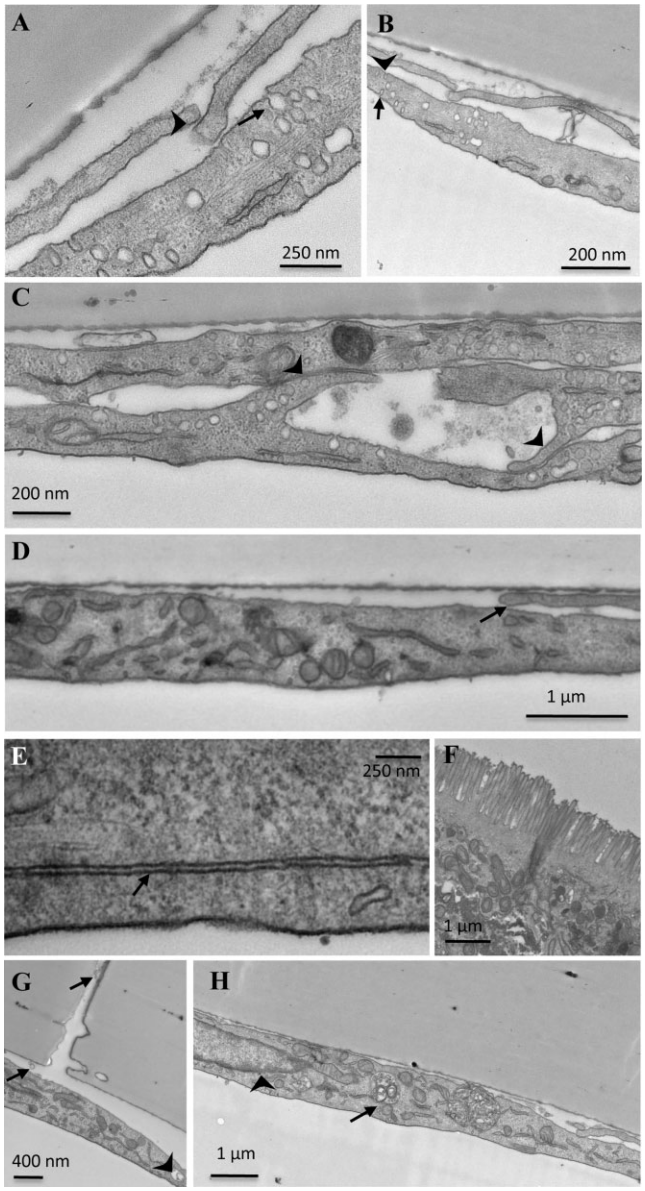

Figure 5. Lipoprotein transcytosis observed within in vitro lymphatic endothelial cells (LECs) in the two-cell model using TEM. **A**: Lipid-containing vesicles (arrow) are seen transcytosing across the LEC even in the proximity of an overlapping junction (arrowhead). **B**: Lipid particle being released on the apical surface of a LEC (arrow) along with a lipid particle entering on the basal surface of the LEC (arrowhead). **C**: Three LECs with overlapping cell junctions (arrowheads) containing lipid vesicles transcytosing through the cells. **D**: In the untreated controls (no OA/TC to promote chylomicron formation by Caco-2 cells), lipid-containing vesicles were rarely seen, while the overlapping junctions (arrow) were similar to those in lipid-transporting cells. **E**: Overlapping junctions (arrow) that are completely closed occur quite regularly, even in the presence of the lipid load. **F**: Microvilli and numerous intracellular vesicles seen on a Caco2 cell in the two-cell model. **G**: Lipid could be seen transporting within a pore in the insert membrane and on the basal side of the LEC (arrows) along with lipid-containing vesicles inside the cell (arrowhead). **H**: Abnormally large vesicles (arrow) containing multiple lipid particles were occasionally seen within LECs (nucleus, arrowhead).

present even in areas of overlapping lymphatic cell edges (Fig. 5A and C, arrowheads).

In contrast, very few lipid-containing vesicles were found in LECs from samples that were not treated with OA/TC (Fig. 5D), which further suggested that the vesicles in OA/TC treated samples contained chylomicrons. Even in the case of OA/TC treated samples, the junctions remain closed with very little gaps as was seen by a high-magnification image of one of these overlapping junctions (Fig. 5E). Brush border-like microvilli on the apical surface of the Caco-2 cells was maintained even after co-culture with LECs (Fig. 5F). Occasionally we observed pores of the insert membrane, where lipid particles were seen within these pores and on the basal side of a LEC (Fig. 5G). Sometimes quite large vesicles were seen transporting multiple chylomicrons or lipoproteins within the cell (Fig. 5H).

There remains uncertainty in the literature as to whether transcellular pathways play major roles in the transport of various particles by lymphatics under normal physiologic conditions. Because of anchoring filaments and a unique valve structure of loosely overlapping cell-cell junctions (Baluk et al., 2007; Leak, 1970, 1971; Trzewik et al., 2001), it is often assumed that lymphatic uptake of fluid and solutes is primarily via paracellular routes; however, lymphatics are known to contain numerous transport vesicles (Azzali, 1999; Feng et al., 2002), and TEM images have shown vesicular transport like that shown in Figure 5. Still, the relative importance of each pathway for fluid, solutes, or chylomicrons and other lipoproteins have not been determined. While further studies are needed to explore this, our model is useful for determining the effects of inhibiting or enhancing transendothelial lipoprotein transport in lymphatics immediately upon secretion by enterocytes.

Conclusions

Tissue engineering has recently made important contributions to elucidating biological mechanisms in a variety of systems (Griffith and Swartz, 2006), including the lymphatics (Griffith and Swartz, 2006; Helm et al., 2005, 2007), although the latter has been to date limited to capillary morphogenesis. Our tissue engineered model of the lacteal is not only be beneficial for elucidating the biology of lipid transport by lymphatics, it can serve as a tool for evaluating the efficacy of drug formulations and delivery systems that target lymphatics for oral drug delivery, which is desirable since it would avoid first-pass clearance in the liver (Porter and Charman, 1997; Porter et al., 2007; Rensen et al., 2001).

Our in vitro model of the lacteal exhibits the most important characteristics relevant to lipid transport of the enterocyte-lymphatic interface in vivo. With this model we can measure the rate of fatty acid and lipid transport from the intestinal lumen to the lumen of the lacteal and can quantify how varying lipid content, lymphatic permeability, or known routes of transcellular transport in endothelial cells alter overall lipid transport. We can also examine the

contributions of each cell type individually to the transport of a species as a whole and quantify the extent that the transport is polarized in the physiologically relevant direction. Using fluorescence imaging we can observe how both paracellular and transcellular transport is utilized by LECs for fatty acid transport, and with TEM we can visualize transcytosis of chylomicrons across LECs, giving us a novel tool to study the regulation of lipid transport and metabolism by LECs. Not only is such a model beneficial for studying some of our basic questions about lymphatic function in lipid trafficking, but it will also be an important tool for evaluating the efficacy of novel nanoparticles for oral drug delivery.

We would like to thank Graham Knott for his invaluable assistance with TEM imaging. This work was supported by NIH (Hl075217 to M.A.S. and K99 KHL091133A to J.B.D.) and the Whitaker International Scholars Fellowship (to J.B.D.).

References

Amenta JS. 1970. A rapid extraction and quantification of total lipids and lipid fractions in blood anf feces. Clin Chem 16(4):339–346.

Azzali G. 1982. The ultrastructural basis of lipid transport in the absorbing lymphatic vessel. J Submicrosc Cytol 14(1):45–54.

Azzali G. 1999. The lymphatic vessels and the so-called 'lymphatic stomata' of the diaphragm: A morphologic ultrastructural and three-dimensional study. Microvasc Res 57(1):30–43.

Baluk P, Fuxe J, Hashizume H, Romano T, Lashnits E, Butz S, Vestweber D, Corada M, Molendini C, Dejana E, et al. 2007. Functionally specialized junctions between endothelial cells of lymphatic vessels. J Exp Med 204(10):2349–2362.

Beckett GJ, Armstrong P, Percy-Robb LW. 1981. A comparison of bile salt binding to lymph and plasma albumin in the rat. Biochim Biophys Acta 664(3):602–610.

Blomstrand R, Dahlback O. 1960. The fatty acid composition of human thoracic duct lymph lipids. J Clin Invest 39(7):1185–1191.

Darimont C, Gradoux N, Cumin F, Baum HP, De Pover A. 1998. Differential regulation of intestinal and liver fatty acid-binding proteins in human intestinal cell line (Caco-2): Role of collagen. Exp Cell Res 244(2):441–447.

Dejana E. 2004. Endothelial cell-cell junctions: Happy together. Nature Rev Mol Cell Biol 5(4):261–270.

Dixon JB, Zawieja DC, Gashev AA, Cote GL. 2005. Measuring microlymphatic flow using fast video microscopy. J Biomed Opt 10(6):064016.

Dixon JB, Moore J, Jr., Coté GL, Gashev AA, Zawieja DC. 2006. Lymph flow, shear stress, and lymphocyte velocity in rat mesenteric prenodal lymphatics. Microcirculation 13:597–610.

Dixon JB, Gashev AA, Zawieja DC, Moore JE, Jr., Cote GL. 2007. Image correlation algorithm for measuring lymphocyte velocity and diameter changes in contracting microlymphatics. Ann Biomed Eng 35(3): 387–396.

Dobbins WO, Rollins EL. 1970. Intestinal mucosal lymphatic permeability—An electron microscopic study of endothelial vesicles and cell junctions. J Ultrastruct Res 33(1–2):29–59.

Feng D, Nagy JA, Dvorak HF, Dvorak AM. 2002. Ultrastructural studies define soluble macromolecular, particulate, and cellular transendothelial cell pathways in venules, lymphatic vessels, and tumor-associated microvessels in man and animals. Microsc Res Tech 57(5):289–326.

Griffith LG, Swartz MA. 2006. Capturing complex 3D tissue physiology in vitro. Nature Rev Mol Cell Biol 7(3):211–224.

Habold C, Reichardt F, Foltzer-Jourdainne C, Lignot JH. 2007. Morphological changes of the rat intestinal lining in relation to body stores depletion during fasting and after refeeding. Pflugers Arch 455(2):323–332.

Harvey NL. 2008. The link between lymphatic function and adipose biology. Ann NY Acad Sci 1131(1):82–88.

Harvey NL, Srinivasan RS, Dillard ME, Johnson NC, Witte MH, Boyd K, Sleeman MW, Oliver G. 2005. Lymphatic vascular defects promoted by Prox1 haploinsufficiency cause adult-onset obesity. Nat Genet 37(10):1072–1081.

Hayashi H, Fujimoto K, Cardelli JA, Nutting DF, Bergstedt S, Tso P. 1990. Fat feeding increases size, but not number, of chylomicrons produced by small-Intestine. Am J Physiol 259(5):G709–G719.

Hayashi H, Sato Y, Kanai S, Ichikawa M, Funakoshi A, Miyasaka K. 2002. Increased lymphatic lipid transport in genetically diabetic obese rats. Am J Physiol Gastrointest Liver Physiol 282(1):G69–G76.

Helm CL, Fleury ME, Zisch AH, Boschetti F, Swartz MA. 2005. Synergy between interstitial flow and VEGF directs capillary morphogenesis in vitro through a gradient amplification mechanism. Proc Natl Acad Sci USA 102(44):15779–15784.

Helm CLE, Zisch A, Swartz MA. 2007. Engineered blood and lymphatic capillaries in 3-D VEGF-fibrin-collagen matrices with interstitial flow. Biotechnol Bioeng 96(1):167–176.

Hosken BD, Cockrill SL, Macfarlane RD. 2005. Metal ion complexes of EDTA: A solute system for density gradient ultracentrifugation analysis of lipoproteins. Anal Chem 77(1):200–207.

Leak LV. 1970. Electron microscopic observations on lymphatic capillaries and the structural components of the connective tissue-lymph interface. Microvasc Res 2(4):361–391.

Leak LV. 1971. Studies on the permeability of lymphatic capillaries. J Cell Biol 50(2):300–323.

Levy E, Mehran M, Seidman E. 1995. Caco-2 cells as a model for intestinal lipoprotein synthesis and secretion. FASEB J 9(8):626–635.

Luchoomun J, Hussain MM. 1999. Assembly and secretion of chylomicrons by differentiated Caco-2 cells. J Biol Chem 274(28):19565–19572.

Mehta D, Malik AB. 2006. Signaling mechanisms regulating endothelial permeability. Physiol Rev 86(1):279–367.

Michel CC, Curry FE. 1999. Microvascular permeability. Physiol Rev 79(3):703–761.

Ng CP, Helm CL, Swartz MA. 2004. Interstitial flow differentially stimulates blood and lymphatic endothelial cell morphogenesis in vitro. Microvasc Res 68(3):258–264.

Orth M, Hanich M, Kröning G, Porsch-Özcürümez M, Wieland H, Luley C. 1998. Fluorometric determination of total retinyl esters in triglyceride-rich lipoproteins. Clin Chem 44(7):1459–1465.

Osada K, Sasaki E, Sugano M. 1994. Lymphatic absorption of oxidized cholesterol in rats. Lipids 29(8):555–559.

Papp M, Makara GB. 1965. The role of the lymph circulation in free fatty acid transport. Experientia 21(12):694.

Pinto M, Robine Leon S, Appay MD. 1983. Enterocyte-like differentiation and polarization of the human colon carcinoma cell line Caco-2 in culture. Biol Cell 47(3):323–330.

Podgrabinska S, Braun P, Velasco P, Kloos B, Pepper MS, Jackson DG, Skobe M. 2002. Molecular characterization of lymphatic endothelial cells. Proc Natl Acad Sci 99(25):16069–16074.

Porter CJH, Charman WN. 1997. Uptake of drugs into the intestinal lymphatics after oral administration. Adv Drug Deliv Rev 25(1):71–89.

Porter CJH, Trevaskis NL, Charman WN. 2007. Lipids and lipid-based formulations: Optimizing the oral delivery of lipophilic drugs. Nature Rev Drug Discov 6(3):231–248.

Rensen PCN, de Vrueh RLA, Kuiper J, Bijsterbosch MK, Biessen EAL, van Berkel TJC. 2001. Recombinant lipoproteins: Lipoprotein-like lipid particles for drug targeting. Adv Drug Deliv Rev 47(2–3):251–276.

Rockson SG. 2004. The elusive adipose connection. Lymphatic Res Biol 2(3):105–106.

Rosen ED. 2002. The molecular control of adipogenesis, with special reference to lymphatic pathology. Ann NY Acad Sci 979:143–158, discussion 188–196.

Rutkowski JM, Moya M, Johannes J, Goldman J, Swartz MA. 2006. Secondary lymphedema in the mouse tail: Lymphatic hyperplasia,

VEGF-C upregulation, and the protective role of MMP-9. Microvasc Res 72(3):161–171.
Ryan TJ. 2006. Adipose tissue and lymphatic function: Is there more to this story especially for tropical diseases? Lymphology 39(1):49–52.
Schmid-Schönbein GW. 1990. Microlymphatics and lymph flow. Physiol Rev 70(4):987–1028.
Thumser AE, Storch J. 2007. Characterization of a BODIPY-labeled fluorescent fatty acid analogue. Binding to fatty acid-binding proteins, intracellular localization, and metabolism. Mol Cell Biochem 299(1–2): 67–73.
Trevaskis NL, Charman WN, Porter CJ. 2008. Lipid-based delivery systems and intestinal lymphatic drug transport: A mechanistic update. Adv Drug Deliv Rev 60(6):702–716.
Trotter PJ, Storch J. 1993. Fatty-acid esterification during differentiation of the human intestinal-cell line Caco-2. J Biol Chem 268(14):10017–10023.
Trzewik J, Mallipattu SK, Artmann GM, Delano FA, Schmid-Schönbein GW. 2001. Evidence for a second valve system in lymphatics: Endothelial microvalves. FASEB J 15(10):1711–1717.
Tso P, Balint JA. 1986. Formation and transport of chylomicrons by enterocytes to the lymphatics. Am J Physiol 250:G715–G726.
Tso P, Balint JA, Rodgers JB. 1980. Effect of hydrophobic surfactant (Pluronic L-81) on lymphatic liquid transport in the rat. Am J Physiol Gastrointest Liver Physiol 2: 5:.
Tso P, Pitts V, Granger DN. 1985. Role of lymph flow in intestinal chylomicron transport. Am J Physiol 249(1):G21–G28.